One-pion exchange model for the reaction $pp \to np\pi^+$ and its verification for pion differential spectra at initial energies from 0.66 to 1.0 GeV

V. K. Suslenko[1)] and I. I. Haysak

Joint Institute for Nuclear Research

(Submitted 18 December 1984)
Yad. Fiz. **43**, 392–404 (February 1986)

A detailed comparison of the available experimental data on the triply differential cross sections $d^3\sigma/dT_\pi^L(q_\pi^L)d\Omega_\pi^L$ for π^+ mesons produced in the reaction $pp \to np\pi^+$ at initial proton energies ~660, 730, 800, 991, and 1000 MeV is performed using an improved version of the one-pion exchange model for this reaction. The model rigorously takes into account the contributions of four Feynman pole diagrams and all their interference terms in the approximation of the 3, 3 resonance for the πN virtual scattering amplitude. The applicability of the model within the ~10–15% accuracy is demonstrated and a pion-nucleon form factor of the form $G(K_i^2) = 9\mu^2/(K_i^2 + 10\mu^2)$ is extracted (here K_i^2 is the squared 4-momentum transferred to the virtual pion in the diagrams with indices $i = 1, 2, 3$, and 4).

INTRODUCTION

Theoretical analyses[1–5] of the reactions of pion production in nucleon-nucleon collisions have successfully used the one-pion exchange model (OPEM), whose main idea is the assumption that to the $NN \to NN\pi$ reactions at energies up to ~3 GeV correspond Feynman pole diagrams with a pion as an intermediate particle.

First comparisons of the OPEM with experiment[1,3] were performed for the differential data of zero order (the total cross sections) and first order (the integrated energy or momentum spectra of the final-state nucleons), primarily for the reaction $pp \to np\pi^+$ at energies in the region 1–3 GeV.

Later, Refs. 4–7 performed the comparison using the experimental data of third order, viz., the differential energy (momentum) spectra at different angles of pions produced in the $pp \to np\pi^+$ reaction at the incident proton energies $T = 654$–670, 730, and 991 MeV. These analyses employed an approximate version of the OPEM which neglects the interference contributions of the diagrams 1, 3 and 2, 4 (see Fig. 1) and for the πN vertices includes only the 3, 3 resonance contribution. From the calculations of Refs. 1 and 6 it follows that the contributions neglected did not exceed ~1–5%. However, this estimate pertains only to the energies above 1 GeV. The question of the interference of the diagrams 1, 3 and 2, 4 in the energy interval 0.6–1 GeV remained open. Exact expressions for these interference terms were derived in Refs. 7–9, and their exact inclusion allowed one to create a unified algorithm for the analysis of the $pp \to np\pi^+$ reactions in the energy region 0.6–1 GeV. In our papers[8,10] this algorithm was implemented as a standard Fortran program which ensures (a) systematic comparison of the theory with the experimental data and (b) detailed analysis of the structure of the OPEM version under study.

The improved OPEM version suggested in Refs. 7 and 8 is used below for the calculation of the differential cross sections of third order for single π^+ mesons produced in the proton-proton collisions

$$p+p \to n+p+\pi^+, \tag{1}$$

taking into account all the contributions of the four Feynman pole diagrams in Fig. 1 (the notations are explained below).

We perform a systematic comparison of the improved OPEM with all the available experimental data of third order, including the new data[11] at the energy $T = 800$ MeV.

1. KINEMATICS OF THE THIRD-ORDER PION SPECTRA

For the reaction (1) the conservation law of the 4-momentum takes the form

$$p_1+p_2=q_2+q_1+q, \tag{1a}$$

where the 4-momenta correspond to the particles as follows: p_1, p_2, and q_1—to the protons, q_2—to the neutron, and q—to the pion (see Fig. 1).

The kinematics of the reactions of the type $2 \to 3$ is described in detail in Refs. 1 and 12. These reactions are characterized by five independent kinematical variables. In particular, one can take the main and the auxiliary sets of the kinematical invariants (in the metric $a^2 = a_0^2 - |\mathbf{a}|^2$):

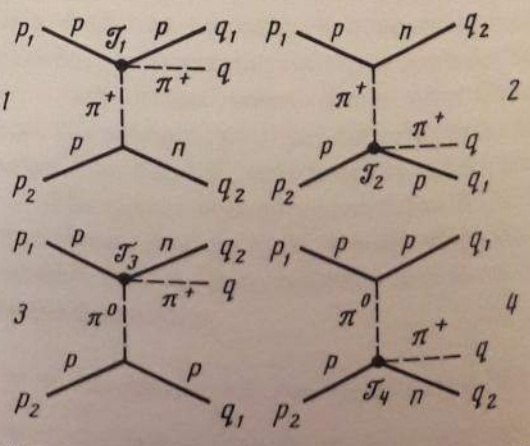

FIG. 1. Feynman pole diagrams corresponding to the reaction (1) in the OPEM.

0038-5506/86/020252-08$03.80

$$W^2=(p_1+p_2)^2,\quad \bar{r}^2=-(q-p_2)^2,\quad r^2=-(q-p_1)^2,$$
$$\Delta^2=-(q_2-p_2)^2,\quad \bar{\Delta}^2=-(q_2-p_1)^2; \tag{2}$$
$$z^2=(q_1+q_2)^2,\quad \omega^2=(q+q_1)^2,\quad u^2=(q+q_2)^2,$$
$$\bar{t}^2=-(q_1-p_2)^2,\quad t^2=-(q_1-p_1)^2. \tag{3}$$

In practical calculations one usually employs the following convenient reference frames S: the lab frame $L(\mathbf{p}_2=0)$, the barycentric frame $B(\mathbf{p}_1+\mathbf{p}_2=0)$, the c.m. frame D of the particles q_1 and q_2, the c.m. frame Q of the particles q and q_1, and the c.m. frame P of the particles q and q_2.

A point in the third-order spectrum of pions produced in the reaction (1) corresponds to fixed values of the three independent variables $T^S(p^S)$, $T_\pi^S(q_\pi^S)$, and θ_π^S, which are produced pion q and the pion polar emission angle in the frame S (in the absence of polarization the dependence on the variable φ_π^S is trivial). These, in turn, correspond to fixed values of three independent invariants W^2, $\bar{r}^2$, and r^2. The remaining independent invariants Δ^2 and $\bar{\Delta}^2$, whose values are free within allowed limits, are conveniently calculated in the D frame (for the polar axis we choose the vector—$\mathbf{p}_2^D$):

$$\Delta^2=2[q_{j0}{}^D p_{20}{}^D-m^2+q_j{}^D p_2{}^D x^D], \tag{4}$$

$$\bar{\Delta}^2=2\{q_{j0}{}^D p_{10}{}^D-m^2-q_j{}^D p_1{}^D[\cos\alpha^D\cdot x^D + \sin\alpha^D\cdot\sqrt{1-x^{D2}}\cos\varphi^D]\}, \tag{5}$$

where for equal proton and neutron masses $m_p=m_n=m$ we have ($j=1$ and 2)

$$q_{j0}{}^D=q_{10}{}^D=q_{20}{}^D=z/2,\quad p_{10}{}^D=(z^2+\bar{r}^2+m^2)/2z,$$
$$p_{20}{}^D=(z^2+r^2+m^2)/2z,$$
$$\cos\alpha^D=\cos(\widehat{\mathbf{p}_1,\ -\mathbf{p}_2})^D=\{W^2-2(m^2+p_{10}{}^D p_{20}{}^D)\}/(2p_1{}^D p_2{}^D) \tag{6}$$

and where

$$x^D=\cos\theta^D=\cos(\widehat{\mathbf{q}_2,\ -\mathbf{p}_2})^D$$

is the polar angle variable and φ^D is the variable of the azimuthal angle between the planes in which lie the vector momenta $\mathbf{q}_2$ and $\mathbf{p}_1$.

The auxiliary invariants (3) are expressed in terms of the main invariants (2) in a simple way and can be used wherever convenient.

The experimental spectra of the final particles are usually given in the frames L or B.

In the L frame for the pions produced in the reaction (1) at the energies

$$T\geqslant\{\mu(4m-\mu)/2(m-\mu)\simeq 316\,\text{MeV}\}$$

(μ is the pion mass) the whole physical interval of angles $-1\leqslant(x_\pi^L=\cos\theta_\pi^L)\leqslant+1$, is allowed: pions emitted into an angle θ_π^L have kinetic energies in the interval $0\leqslant T_\pi^L\leqslant T_\pi^{L\max}(x_\pi^L)$, where (omitting the index L)

$$T_\pi^{max}(x_\pi)=\{2[(2m+T)^2-p^2x_\pi{}^2]\}^{-1}\{(2m+T)(2mT+\mu^2)+px_\pi \times[(2mT+\mu^2)^2-4\mu^2[(2m+T)^2-p^2x_\pi{}^2]]^{1/2}\}-\mu, \tag{7}$$

while in the B frame the allowed interval of pion emission angles and their energy spectrum for each allowed angle $\theta_\pi^B(x_\pi^B=\cos\theta_\pi^B)$ are

$$\left.\begin{aligned}&-1\leqslant x_\pi{}^B\leqslant+1,\\ &0\leqslant T_\pi{}^B\leqslant\{T_\pi{}^{B\,max}=[(W-\mu)^2-4m^2]/2W\}.\end{aligned}\right\} \tag{8}$$

2. GENERAL EXPRESSION FOR THE DIFFERENTIAL CROSS SECTION

The purpose of the present application of the one-pion exchange model to the reaction (1) and, specifically, of the computer code OPEM-3 (Refs. 8 and 10) is the calculation of the differential cross section of third order for the pions produced in the reaction (1). The general expression for this cross section has the form (see Refs. 1–4, 7 and 8)

$$\frac{d^3\sigma}{dT_\pi{}^S dx_\pi{}^S d\varphi_\pi{}^S}$$
$$=\frac{m^4}{2(2\pi)^5}\frac{|\mathbf{q}_\pi{}^S|}{F}\left\{\frac{q_j{}^D}{z}\right\}\int_0^{2\pi}d\varphi^D\int_{-1}^{+1}U(X_\pi{}^S;x^D,\varphi^D)dx^D, \tag{9}$$

where the superscript S stands for any reference frame, $F=[(p_1\cdot p_2)^2-m_1^2m_2^2]^{1/2}$ is the invariant flux, while the integrand $U(X_\pi^S;x^D,\varphi^D)$ is the squared total matrix element of all the diagrams of Fig. 1, summed over the final states and averaged over the initial states; X_π^S is the set of fixed variables $T_\pi^S(q_\pi^S)$, x_π^S, and φ_π^S; x^D, and φ^D play the role of the integration variables.

In the matrix element of a given diagram with the index i we separate out two factors associatated with the πN scattering amplitude and the πNN vertex:

$$\mathscr{M}_i\sim\{\mathscr{T}(z_i,y_i^2;K_i^2)\}\cdot\Pi(K_i^2),\quad i=1,2,3,4, \tag{10}$$

where z_i is the total energy of the πN system, y_i^2 is the squared 4-momentum transferred in πN virtual scattering, and K_i^2 is the squared 4-momentum of the virtual pion.

Below we study in detail the structure of these factors, which is necessary in order to establish the explicit form of the integrand function $U(X_\pi^S;x^D,\varphi^D)$.

3. πN VIRTUAL SCATTERING AMPLITUDE

The amplitude for πN virtual scattering $\mathscr{T}_i=\mathscr{A}_i+\hat{q}\mathscr{B}_i$ and its off-mass-shell behavior is described on the basis of Ref. 2, where the virtuality corrections are introduced into the partial waves. The invariant amplitudes $\mathscr{A}_i$ and $\mathscr{B}_i$, which enter into $\mathscr{T}_i$, are written in terms of the helicity amplitudes f_1 and f_2 in analogy with physical πN scattering:

$$\mathscr{A}_i(z_i,y_i{}^2;K_i^2)=4\pi\left[\frac{z_i+m}{R_i^{(+)}}f_1(z_i,y_i{}^2;K_i^2)-\frac{z_i-m}{R_i^{(-)}}f_2(z_i,y_i{}^2;K_i^2)\right],$$
$$\mathscr{B}_i(z_i,y_i{}^2;K_i^2)=4\pi\left[\frac{1}{R_i^{(+)}}f_1(z_i,y_i{}^2;K_i^2)+\frac{1}{R_i^{(-)}}f_2(z_i\ y_i{}^2;K_i^2)\right] \tag{11}$$

TABLE I.

i	1: Variables with the index i and indices i and S.									
	z_i^2	y_i^2	K_i^2	$c_i^{3/2}$	S	$\cos\theta_i^S$	a_{i0}^S	a_i^S	b_{i0}^S	b_i^S
1	ω^2	t^2	Δ^2	$\sqrt{2}$	Q	$\cos\theta^Q$	$p_{10}{}^Q$	$p_1{}^Q$	$q_{10}{}^Q$	$q_1{}^Q$
2	ω^2	$\bar{t}^2$	$\bar{\Delta}^2$	$\sqrt{2}$	Q	$\cos\varepsilon^Q$	$p_{20}{}^Q$	$p_2{}^Q$	$q_{10}{}^Q$	$q_1{}^Q$
3	u^2	$\bar{\Delta}^2$	$\bar{t}^2$	$-\sqrt{2}/3$	P	$\cos\varepsilon^P$	$p_{10}{}^P$	$p_1{}^P$	$q_{20}{}^P$	$q_2{}^P$
4	u^2	Δ^2	t^2	$-\sqrt{2}/3$	P	$\cos\theta^P$	$p_{20}{}^P$	$p_2{}^P$	$q_{20}{}^P$	$q_2{}^P$

where

$$R_i^{(\pm)}=[(a_{i0}{}^S\pm m)(b_{i0}{}^S\pm m)]^{1/2}, \tag{12}$$

while a_{i0}^S and b_{i0}^S are the total energies of the initial and final nucleons.

Assuming that the πN scattering is dominated by the 3, 3 resonance,[1] one has

$$f_1(z_i, y_i^2; K_i^2)\simeq c_i^{1/2}\cdot 3\cos\theta_i^S\cdot f_{1+}^{1/2}(z_i; K_i^2),$$
$$f_2(z_i, y_i^2; K_i^2)\simeq -c_i^{1/2}f_{1+}^{1/2}(z_i; K_i^2), \tag{13}$$

where $c_i^{3/2}$ are the isospin coefficients of the diagrams of Fig. 1 corresponding to the 3, 3 resonance, θ_i^S is the angle between the initial and final nucleon momenta in the πN scattering, whose value is given by the expression

$$\cos\theta_i^S=[2a_{i0}{}^Sb_{i0}{}^S-2m^2-y_i^2]/2a_i^Sb_i^S, \tag{14}$$

and $f_{1+}^{3/2}(z_i;K_i^2)$ is the 3, 3 partial off-mass-shell amplitude. The values of these quantities for different values of the index i in a frame S are listed in Table I.

The expression for the 3, 3 partial off-mass-shell amplitude $f_{33}(z_i; K_i^2)$ ($f_3\equiv f_{1+}^{3/2}$), obtained in Ref. 2 on the basis of the dispersion relations, has the form

$$f_{33}(z_i; K_i^2)=\frac{f_{33}{}^B(z_i; K_i^2)}{f_{33}{}^B(z_i; -\mu^2)}f_{33}(z_i; -\mu^2), \tag{15}$$

where

$$f_{33}{}^B(z_i; K_i^2)\sim\left[\frac{z_i-m}{2z_iR_i^{(-)}}Q_1(\beta_i)-\frac{z_i+m}{2z_iR_i^{(+)}}Q_2(\beta_i)\right] \tag{16}$$

is the Born term of the off-mass-shell 3, 3 amplitude, the quantities $R_i^{(\pm)}$ are defined in (12), $Q_l(\beta_i)$ are the Legendre functions of the second kind of order l of the argument

$$\beta_i\equiv\beta(z_i)=[2a_{i0}{}^S(z_i-b_{i0}{}^S)-\mu^2]/2a_i^Sb_i^S, \tag{17}$$

and the ratio

$$\Gamma(K_i^2)=f_{33}{}^B(z_i;\ K_i^2)/f_{33}{}^B(z_i;\ -\mu^2) \tag{18}$$

is the off-mass-shell correction factor which is practically independent of the energy z_i (Ref. 2).

The physical 3, 3 πN partial scattering amplitude can be given in the Breit-Wigner form[13]

$$f_{33}(z_i)=\frac{1}{2b_i^S}\gamma[(z^*-z_i)-i\gamma/2]^{-1} \tag{19}$$

where

$$\gamma=\gamma_0\cdot 2(ab_i^S)^3/[1+(ab_i^S)^2] \tag{20}$$

with the following parameter values: $z^*=1232$–1238 MeV, $a=6.3\cdot10^{-3}$ MeV^{-1}, and $\gamma_0=58$ MeV.

4. FORM FACTOR OF THE πNN VERTEX

In the expression (10) the factor

$$\Pi(K_i^2)=\frac{1}{K_i^2+\mu^2}\cdot G(K_i^2) \tag{21}$$

is the product of the propagator of the intermediate pion $1/(K_i^2+\mu^2)$ with the so-called pion-nucleon form factor $G(K_i^2)$ which in the OPEM is not defined. The form of $G(K_i^2)$ can be established by comparison with experiment at some fixed energy since in the case of one-pion exchange dominance the form factor depends only on the momentum transfer K_i^2 and is independent of the initial energy T (Ref. 1). Refs. 2–8 established that the function

$$G(K_i^2)=\bar{A}\mu^2/[K_i^2+(\bar{A}+1)\mu^2] \tag{22}$$

with $\bar{A}=8$–9 gives a sufficiently good description of the experimental data in the energy region $T=0.66$–1 GeV.

5. THE FUNCTION $U(X_\pi^S; x^D, \varphi^D)$—THE SQUARED MATRIX ELEMENT OF THE ONE-PION EXCHANGE MODEL FOR THE REACTION (1)

The total matrix element $\mathcal{M}$ for the reaction (1) is given by the following algebraic sum of the matrix elements of the diagrams of Fig. 1:

$$\mathcal{M}=\mathcal{M}_1-\mathcal{M}_2-\mathcal{M}_3+\mathcal{M}_4, \tag{23}$$

where the minus signs stem from the Pauli principle taking into account the isotopic invariance of the strong interactions.

The standard procedure of calculation of the trace $\mathrm{Sp}\mathcal{M}\mathcal{M}^+$ leads to the following form of the integrand in (9):

$$U=\tfrac{1}{4}\,\mathrm{Sp}\,\mathcal{M}\mathcal{M}^+=\sum_{i=1}^{4}T_i+(_1T_2+{}_3T_4)+(_1T_3+{}_2T_4), \tag{24}$$

where the first term is a sum of squared matrix elements of the separate diagrams of Fig. 1, while the other terms represent the interference of the corresponding diagrams. Because of pseudoscalarity of the pion, the interference of the diagrams 1, 4 and 2, 3 yields zero. For clarity the structure of the squared total matrix element is schematically depicted in Fig. 2.

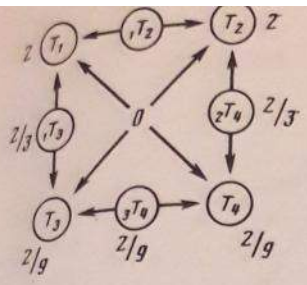

FIG. 2. The scheme of the contributions of the diagrams of Fig. 1 corresponding to the reaction (1) in the OPEM. The contributions T_i ($i = 1, 2, 3$, and 4) are squared matrix elements of separate diagrams; the contributions ${}_iT_j$ ($i, j = 1, 2, 3$, and 4; $i \neq j$) are the interference terms of the diagrams i and j. The numbers correspond to the isotopic weights of the diagrams in the squared total matrix element of the reaction (see Table I).

The squared matrix elements of the separate diagrams of Fig. 1 have the form ($i = 1, 2, 3$, and 4)

$$T_i = \frac{1}{16m^4} G_r^2 \Pi_i^2 K_i^2 \{(y_i^2+4m^2)\mathscr{A}_i^2 + 2m[2(z_i^2-m^2) + (K_i^2-y_i^2-\mu^2)]\,\mathrm{Re}\,(\mathscr{A}_i\mathscr{B}_i^*) + [(z_i^2-m^2-\mu^2)(z_i^2+K_i^2-m^2) - y_i^2(z_i^2-m^2)]\mathscr{B}_i^2\}, \quad (25)$$

where G_r^2 is the renormalized strong-interaction coupling constant: $G_r^2 = 16\pi(m/\mu)^2 f^2$, and $f^2 = 0.08$.

The contribution of the interference of the diagrams 1 and 2 is given by the expression

$$ {}_1T_2 = G_r^2 \Pi_1 \Pi_2 \{I_{12}^{\mathscr{A}\mathscr{A}}\,\mathrm{Re}\,(\mathscr{A}_1 A_2^*) + I_{12}^{\mathscr{A}\mathscr{B}}\,\mathrm{Re}\,(\mathscr{A}_1\mathscr{B}_2^*) + I_{12}^{\mathscr{B}\mathscr{A}}\,\mathrm{Re}\,(\mathscr{B}_1\mathscr{A}_2^*) + I_{12}^{\mathscr{B}\mathscr{B}}\,\mathrm{Re}\,(\mathscr{B}_1\mathscr{B}_2^*)\}, \quad (26)$$

where

$$I_{12}^{\mathscr{A}\mathscr{A}} = \frac{1}{8m^2}\{(m^2+p_1p_2+q_1p_2+q_1p_1-q_2p_1-q_2p_2-q_1q_2) + \frac{1}{m^2}(q_1q_2\cdot p_1p_2 - q_1p_2\cdot q_2p_1 - q_1p_1\cdot q_2p_2)\}$$
$$= \frac{1}{8m^4}\{2(q_1p_1\cdot q_1p_2 - m^2\cdot q_1q_2) - (m^2\cdot qq_2 + qq_1\cdot p_1p_2) + (qp_1\cdot q_1p_2 + qp_2\cdot q_1p_1)\}, \quad (27)$$

$$I_{12}^{\mathscr{A}\mathscr{B}} = \frac{1}{8m}\{(\mu^2+2qq_1) + \frac{1}{m^2}[qq_1(-q_2p_1-q_2p_2+p_1p_2) + qq_2(-q_1p_1+q_1p_2+p_1p_2) + qp_1(q_1q_2-q_1p_2-q_2p_2) + qp_2(-q_1q_2+q_1p_1-q_2p_1)]\} \quad (28)$$

$$I_{12}^{\mathscr{B}\mathscr{A}} = \frac{1}{8m}\{(\mu^2+2qq_1) + \frac{1}{m^2}[qq_1(-q_2p_1-q_2p_2+p_1p_2) + qq_2(q_1p_1-q_1p_2+p_1p_2) + qp_1(-q_1q_2+q_1p_2-q_2p_2) + qp_2(q_1q_2-q_1p_1-q_2p_1)]\}, \quad (29)$$

$$I_{12}^{\mathscr{B}\mathscr{B}} = \frac{1}{8m^2}\{\mu^2[(m^2+p_1p_2+q_1q_2-q_1p_1-q_1p_2-q_2p_1-q_2p_2) + \frac{1}{m^2}(q_1p_1\cdot q_2p_2+q_1p_2\cdot q_2p_1-q_1q_2\cdot p_1p_2)] + 2qq_1[(\mu^2+qq_1) + \frac{1}{m^2}(qq_2\cdot p_1p_2 - qp_1\cdot q_2p_2 - qp_2\cdot q_2p_1)]\}. \quad (30)$$

The contribution of the interference of the diagrams 3 and 4 is obtained from (26) by the subscript replacement $1\to3$ and $2\to4$ with the simultaneous interchange $q_1 \rightleftarrows q_2$ everywhere in the expressions (27)–(30).

The contribution of the interference of the diagrams 1 and 3 is given by the expression

$$ {}_1T_3 = G_r^2 \Pi_1 \Pi_3 \{I_{13}^{\mathscr{A}\mathscr{A}}\,\mathrm{Re}\,(\mathscr{A}_1\mathscr{A}_3^*) + I_{13}^{\mathscr{A}\mathscr{B}}\,\mathrm{Re}\,(\mathscr{A}_1\mathscr{B}_3^*) + I_{13}^{\mathscr{B}\mathscr{A}}\,\mathrm{Re}\,(\mathscr{B}_1\mathscr{A}_3^*) + I_{13}^{\mathscr{B}\mathscr{B}}\,\mathrm{Re}\,(\mathscr{B}_1\mathscr{B}_3^*)\},$$

where

$$I_{13}^{\mathscr{A}\mathscr{A}} = \frac{1}{8m^2}\{(m^2+q_1p_1+q_2p_1+q_1q_2-q_1p_2-q_2p_2-p_1p_2) + \frac{1}{m^2}(q_1q_2\cdot p_1p_2 - q_1p_1\cdot q_2p_2 - q_1p_2\cdot q_2p_1)\}$$
$$= \frac{1}{8m^4}\{2(q_1p_1\cdot q_2p_1 - m^2\cdot p_1p_2) + (m^2\cdot qp_2 + qp_1\cdot q_1q_2) - (qq_1\cdot q_2p_1 + qq_2\cdot q_1p_1)\}, \quad (31)$$

$$I_{13}^{\mathscr{A}\mathscr{B}} = \frac{1}{8m}\{(-\mu^2+2qp_1) + \frac{1}{m^2}[qq_1(-q_2p_1-q_2p_2+p_1p_2) + qq_2(q_1p_1-q_1p_2-p_1p_2) + qp_1(q_1q_2-q_1p_2-q_2p_2) + qp_2(q_1q_2-q_1p_1+q_2p_1)]\}, \quad (32)$$

$$I_{13}^{\mathscr{B}\mathscr{A}} = \frac{1}{8m}\{(-\mu^2+2qp_1) + \frac{1}{m^2}[qq_1(q_2p_1-q_2p_2-p_1p_2) + qq_2(-q_1p_1-q_1p_2+p_1p_2) + qp_1(q_1q_2-q_1p_2-q_2p_2) + qp_2(q_1q_2+q_1p_1-q_2p_1)]\}, \quad (33)$$

$$I_{13}^{\mathscr{B}\mathscr{B}} = \frac{1}{8m^2}\{\mu^2[(m^2+p_1p_2+q_1q_2-q_1p_1-q_1p_2-q_2p_1-q_2p_2) + \frac{1}{m^2}(q_1p_1\cdot q_2p_2+q_1p_2\cdot q_2p_1-q_1q_2\cdot p_1p_2)] + 2qp_1[(-\mu^2+qp_1) + \frac{1}{m^2}(qp_2\cdot q_1q_2 - qq_1\cdot q_2p_2 - qq_2\cdot q_1p_2)]\}. \quad (34)$$

The contribution of the interference of the diagrams 2 and 4 is obtained from (31) by the subscript replacement $1\to2$ and $3\to4$ with the simultaneous interchange $p_1 \rightleftarrows p_2$ everwhere in the expressions (32)–(35).

Since the scalar products in terms of which the quantities (26)–(35) are written can be expressed through the kinematical invariants (2), the above formulae give a complete and detailed account of the OPEM version used in our computer code OPEM-3 for the calculation of the differential cross sections of third order for pions produced in the reaction (1).

6. COMPARISON OF THE RESULTS CALCULATED USING THE COMPUTER CODE OPEM-3 WITH THE EXPERIMENTAL DATA

The expression (9), which contains the exact expressions for the squared OPEM matrix elements (25)–(35), is represented as the following sum:

TABLE II. Absolute values in the maxima of the theoretical and experimental differential energy spectra presented in Fig. 3.

T, MeV	θ_π^L, deg	Ref	$d^3\sigma/dT_\pi^L d\Omega_\pi^L$, 10^{-31} cm^2/(MeV·sr)		
			experiment	OPEM-3	
				$\overline{A}=9$	$\overline{A}=8$
670	19,5	[14]	2,37±0,26	2,40	2,11
657	24	[15]	relat. units	1,93	1,69
655	30	[16]	1,65±0,23	1,47	1,28
670	38	[14]	1,57±0,13	1,12	0,97
660	46	[17]	1,33±0,33	0,85	0,74
670	56	[14]	1,30±0,14	0,74	0,65
654		[18]	0,80±0,04	0,70	0,61
660	108	[19]	1,00±0,18	0,84	0,73
660	123	[19]	1,07±0,12	0,90	0,79
660	140	[19]	0,92±0,10	0,92	0,81
660	160	[19]	0,92±0,10	0,96	0,86

$$
{}^3\sigma_\pi = \frac{d^3\sigma}{dT_\pi{}^B\, dx_\pi{}^B\, d\varphi_\pi{}^B} = \frac{m^4}{2(2\pi)^5}\frac{|\mathbf{q}_\pi{}^B|}{F}
$$

$$
\times\left\{\frac{q_j{}^D}{z}\right\}\int_0^{2\pi} d\varphi^D \int_{-1}^{+1}[(T_1+T_3)+(T_2+T_4)
$$

$$
+({}_1T_2+{}_3T_4)+({}_1T_3+{}_2T_4)]\,dx^D
$$

$$
=A+B+C+D=ABCD,
$$

which is convenient for separating out the characteristic contributions to ${}^3\sigma_\pi$.

The earlier papers[1-7] (with the partial exception of Ref. 6) have only calculated the contributions ABC.

In the present paper, on the basis of the explicit expressions (31)–(35), we rigorously take into account the interferences $D\sim {}_1T_3+{}_2T_4$, calculate the quantities ${}^3\sigma_\pi = ABCD$, and perform a detailed comparison of them with the available experimental data at the energies

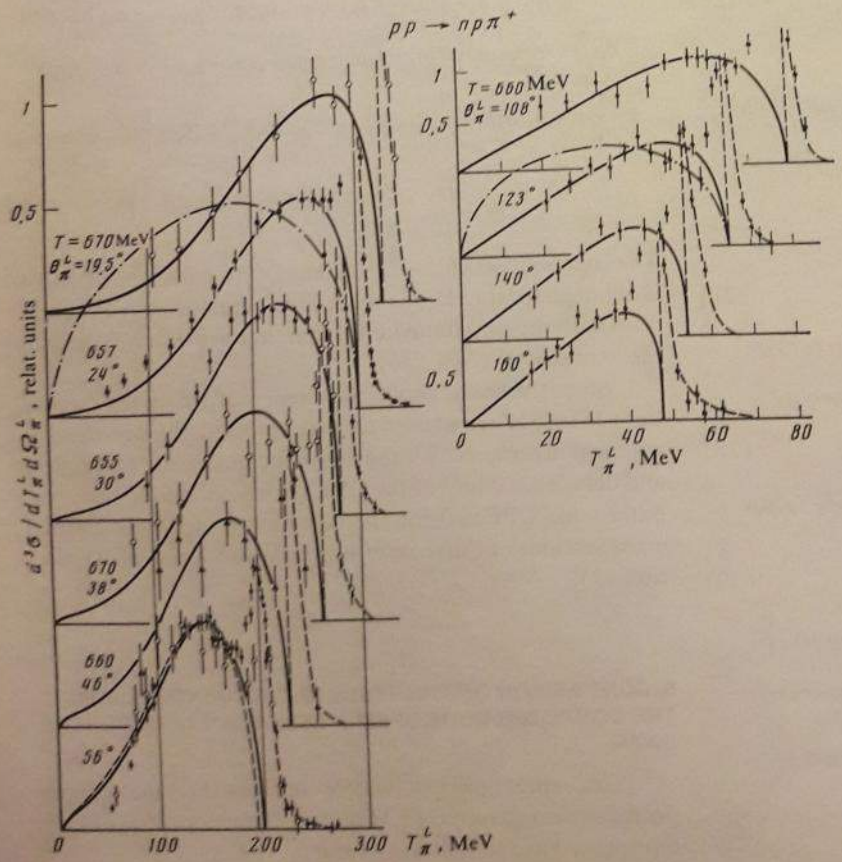

FIG. 3. Comparison of the theoretical and experimental differential energy distributions (third-order spectra) in the L frame for pions produced in the $pp\to np\pi^+$ reaction at the initial energies $T = 654$–670 MeV and pion-emission angles $\theta_\pi^L = 19.5$, 24, 30, 38, 46, 56, and 108° (left-hand side of the figure) and $\theta_\pi^L = 108$, 123, 140, and 160° (right-hand side of the figure). The solid curves are calculated in the present paper using the OPEM-3 code with the form factors $G(K_i^2) = 9\mu^2/(K_i^2 + 10\mu^2)$ and the off-mass-shell correction $\Gamma(K_i^2)$ given by the formula (18). The dot-dashed curves at $\theta_\pi^L = 24$ and 123° show the behavior of the phase-space volume. The solid curve at $\theta_\pi^L = 56°$ corresponds to $T = 670$ MeV, and the dashed curve corresponds to $T = 654$ MeV. The experimental points are as follows: ○—Ref. 14, ■—Ref. 15, ●—Refs. 16, 18, and 19, and ▲—Ref. 17. The dashed lines indicate the position of the boundary of the pion spectra in the reaction $pp\to np\pi^+$ and the behavior of the right-hand-side falloff of the peak in the pion spectra in the reaction $pp\to d\pi^+$. All the calculated curves and the experimental data are normalized to unity at their maxima. The actual absolute values can be reconstructed from their values at the maxima presented in Table II.

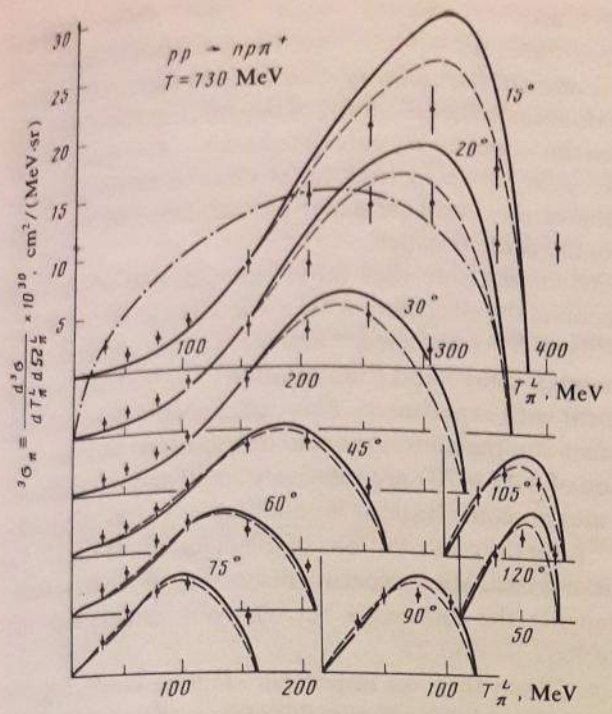

FIG. 4. Same as in Fig. 3 for $T = 730$ MeV and $\theta_\pi^L = 15, 20, 30, 45, 60, 75, 90, 105$, and 120° in the L frame. The solid curves include all the contributions $ABCD$ to ${}^3\sigma_\pi$; the dashed curves include the contributions ABC (omitting the contribution D of the interference of the diagrams 1, 3 and 2, 4 of Fig. 1); the dot-dashed curve depicts the phase-space volume. The experimental points ● are from Ref. 5. All the calculated curves (except the phase-space one) and the experimental data are given in absolute units.

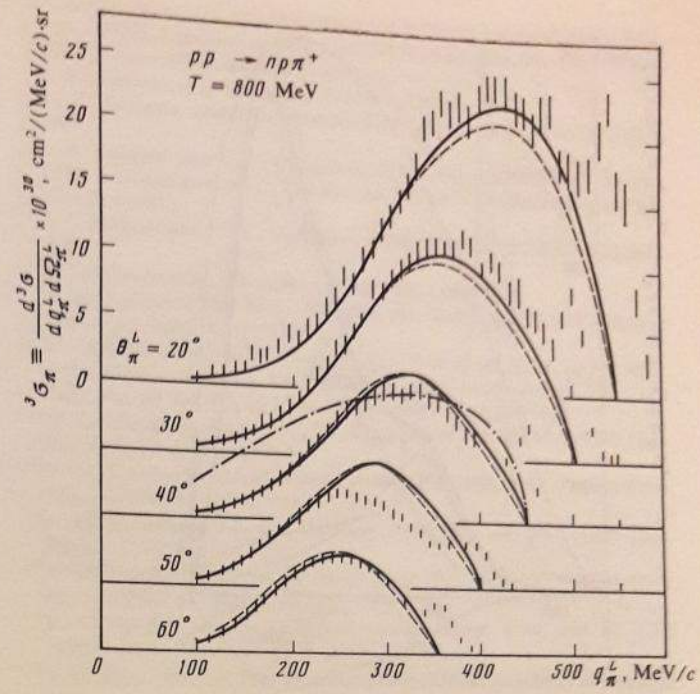

FIG. 5. Same as in Fig. 4 at $T = 800$ MeV for the differential momentum spectra ${}^3\sigma_\pi$ in the L frame for pion-emission angles $\theta_\pi^L = 20, 30, 40, 50$, and 60°. The vertical dashes are the experimental data of Ref. 11. All the calculated curves (except the phase-space one) and the experimental data are given in absolute units.

$T = 654$–670, 730, 800, 991, and 1000 MeV. The results are presented in Figs. 3–8. It is important to note that the absolute values of the contributions D to ${}^3\sigma_\pi$ depend on the initial energy T of the reaction (1) and on the pion-emission angle θ_π^L; in the forward hemisphere, with decrease of these quantities the contribution D grows. In particular, this dependence on the energy T, depicted in Fig. 8 for the angle $\theta_\pi^L = 20°$, results in the relative values of the D contribution ~12, 6 and 2.5% for, respectively, $T = 670$, 800, and 991 MeV. The dependence of D on the pion-emission angle $\theta_\pi^{L,B}$ is partially reflected in Figs. 4–6.

7. CONCLUSIONS AND DISCUSSION

The general result of the comparison of our calculations with the available experimental data for ${}^3\sigma_\pi$ at the energies $T = 654$–670, 800, and 991 MeV is good agreement with

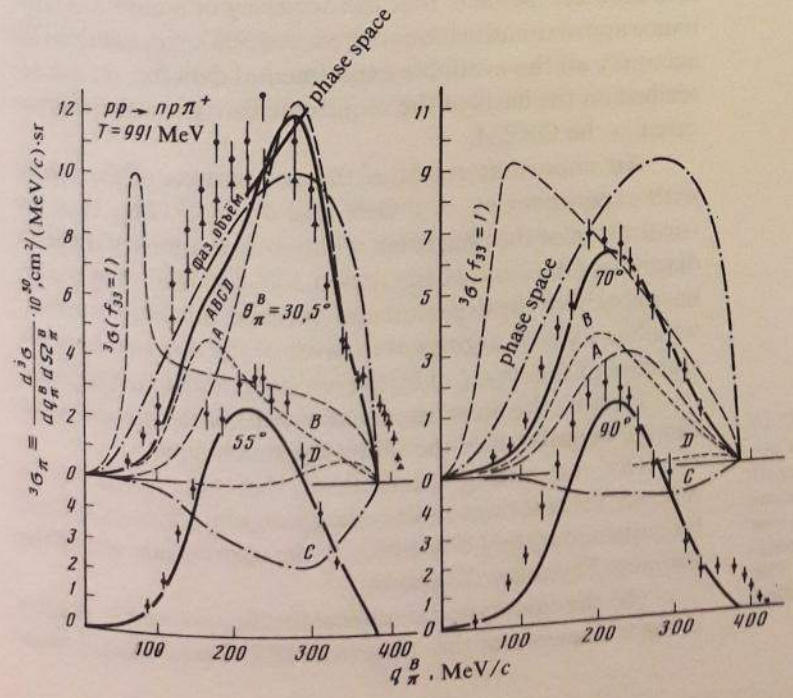

FIG. 6. Differential momentum spectra of pions in the reaction (1) at $T = 991$ MeV, presented in the frame $B(\mathbf{p}_1 + \mathbf{p}_2 = 0)$ for the angles $\theta_\pi^B = 30.5$, 55, 125°, 70 and 110, and 90°. The solid curves include all the contributions $ABCD$. The dashed curves A, B, C, and D give the separate contributions $A \sim T_1 + T_3$, $B \sim T_2 + T_4$, $C \sim {}_1T_2 + {}_3T_4$, and $D \sim {}_1T_3 + {}_2T_4$; the dashed curve ${}^3\sigma(f_{33} = 1)$ shows the behavior of the cross section ${}^3\sigma_\pi$ when the πN 3, 3 scattering amplitude is set equal to unity everywhere. All the calculated curves (except the $\varepsilon\sigma_\pi$ with $f_{33} = 1$ and the phase-space curve) and the experimental data are given in absolute units. The experimental points ● and ▲ are taken from Ref. 6.

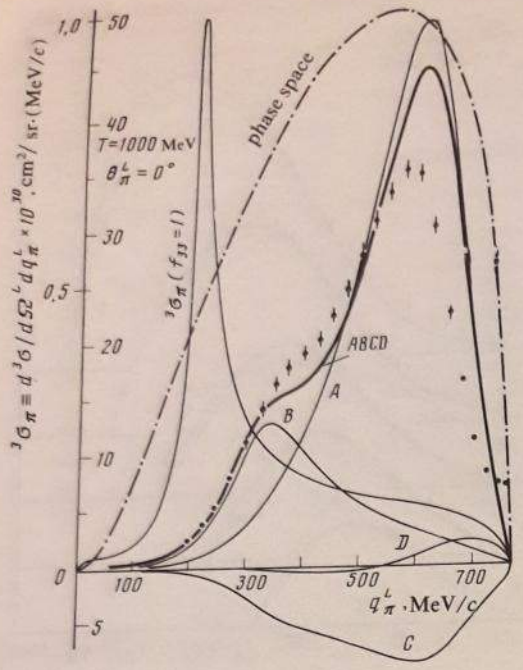

FIG. 7. Differential momentum spectrum of pions emitted into the angle $\theta_\pi^L = 0°$ in the $pp \to np\pi^+$ reaction at the initial energy $T = 1000$ MeV. The thick solid curve (which includes all the contributions $ABCD$ to $^3\sigma_\pi$), the thin solid curves (for separate contributions A, B, C, and D), and the experimental data are given in absolute units; the curve for $^3\sigma_\pi$ with $f_{33} = 1$ and the phase-space curve (the dot-dashed curve) are normalized to unity. The experimental points are taken from Ref. 20.

experiment of our version of the OPEM with the form factor $G(K_i^2) = g\mu^2/(K_i^2 + 10\mu^2)$. For the $T = 730$ MeV data the form of the spectra is reproduced well but better absolute

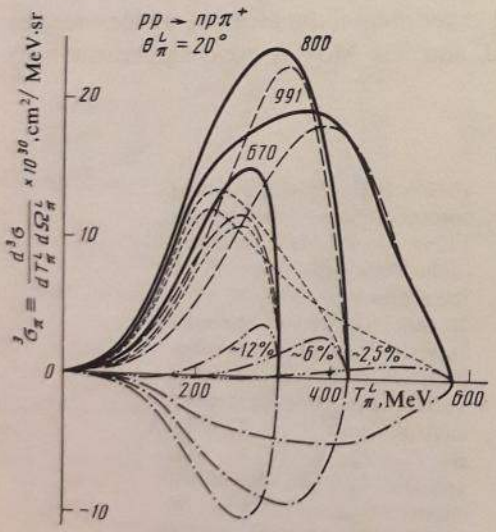

FIG. 8. Differential energy spectra of pions in the reaction $pp \to np\pi^+$ in the L frame for $T = 670$ 800, and 991 MeV and $\theta_\pi^L = 20°$, and their decomposition into separate contributions. The thick solid curve includes all the contributions $ABCD$, the long-dash curve shows the contribution $A \sim T_1 + T_3$, the short-dash curve shows $B \sim T_2 + T_4$, the dot-dash curve shows $C \sim {}_1T_2 + {}_3T_4$, and double-dot-dashed curve shows the contribution $D \sim {}_1T_3 + {}_2T_4$. All the calculated curves are in absolute units. The magnitude of the contributions D is indicated under the corresponding curves.

values are obtained with the form factor $G(K_i^2) = 8\mu^2/(K_i^2 + 9\mu^2)$. Numerous calculations show that variation of the quantity $\bar{A}$ in the form factor (22) practically does not affect the form of the spectra; the difference between the values of $^3\sigma_\pi$ calculated with $\sim A = 8$ and $\bar{A} = 9$ is of the order 10% and, thus, lies within the overall limits of accuracy of the available experimental data for $^3\sigma_\pi$, analyzed in the present paper.

One should note that other calculations, which take into account the diagrams with the exchange of the ρ mesons[21,22] and N^* resonance,[22] and include the contributions of the nonresonant S and P amplitudes,[11,22] also lead to good agreement with experiment. This can probably be explained by the fact that the nonresonance contributions and the contribution of $N^*(1470)$ are relatively small and, in addition, the ρ-meson contribution is qualitatively indistinguishable[21,22] from the contributions of the diagrams of Fig. 1. An analysis of polarization experiments would, obviously, facilitate gauging the difference between our calculation and those of Refs. 11 and 21.

Apart from that, an important stage in clarifying the degree of applicability of the OPEM to the reaction (1) should be a systematic analysis of kinematically complete experiments in which (any) two of the three final particles are detected in coincidence. The first such experiment,[22] where the p and π^+ in the reaction (1) were detected in coincidence, allows one to begin an analysis of this kind even though the measurement set there is very limited and definite conclusions cannot yet be drawn.

One can assume that future studies will better determine the degree of applicability of the basic assumptions of the OPEM about the dominance of the pole Feynman diagrams (Fig. 1) and existence (in the region of applicability of this model) of a unified form-factor function of the form $\mathcal{L}(K_i^2) = \Gamma(K_i^2) \cdot G(K_i^2)$ which depends only on the momentum transfer K_i^2 and is independent of the initial energy T. Nevertheless, the results of the present paper allow one to think that these improvements will not exceed 20% (taking into account the fact[6] that the accuracy of a pure 3, 3 resonance approximation does not exceed 5%), since within this accuracy all the available experimental data for $^3\sigma_\pi$ are described on the basis of the requirements rigorously incorporated in the OPEM.

An important result of the comparison of the theory with experiment at $= 1$ GeV and $\theta_\pi^L = 0°$ (Fig. 7) is the verification of the character of the contributions of different diagrams (the bend in the region 300–500 MeV/c in the behavior of both the experimental data and calculated curves), which is a visual argument in favor of the description of the reaction of the type (1) by the one-pion exchange diagrams.

Finally, the most important results of the present paper can be formulated in the following statements:

(a) the strong interactions that take place in the $NN \to NN\pi$ reactions in the energy region ~ 0.6–1 GeV can be quite accurately described by the appropriate sets of the simplest Feynman diagrams;

(b) the calculational scheme for the $pp \to np\pi^+$ reaction in the framework of the suggested OPEM version ensures an

accuracy which exceeds the current experimental capabilities; this scheme, thus, can certainly be used as an ingredient in the calculations of nucleon-nucleus and nucleus-nucleus collisions (for instance, in intranucleus cascade calculations).

To conclude, the authors express their sincere gratitude to V. P. Dzhelepov, M. G. Mescheryakov, K. O. Oganesyan, N. A. Perfilov, O. V. Lozhkin, V. A. Meshcheryakov, and V. G. Kadyshevskiĭ for making it possible to perform this work and for their interest in it. One of us (V. K. S.) thanks E. Ferrari and F. Selleri for correspondence, their attention, and interest in his work.

[1]V. G. Khlopin Radium Institute, Leningrad.

[1]E. Ferrari and F. Selleri, Nuovo Cimento **27**, 1450 (1963); Suppl. Nuovo Cimento **24**, 453 (1962).
[2]F. Selleri, Nuovo Cimento **40A**, 236 (1965); F. Selleri, in: *Lect. in Theor. Phys.* **7B** (1965) (Univ. of Colorado Press, eds. W. E. Brittin and L. Marshall), p. 183.
[3]U. Amaldi, Jr., R. Biancastelli, and S. Francaviglia, Nuovo Cimento **47A**, 85 (1967).
[4]V. K. Suslenko and V. I. Kochkin, JINR Preprint P2-5572, Dubna, 1971.
[5]D. R. F. Cochran *et al.*, Phys. Rev. D **6**, 3085 (1972).
[6]V. G. Vovchenko *et al.*, LIYaF Preprint #213 (Leningrad Nucl. Phys. Inst., USSR Academy of Sciences), 1976. Yad. Fiz. **24**, 1161 (1976) [Sov. J. Nucl. Phys. **24**, 608 (1976)].
[7]V. K. Suslenko, JINR Preprint 2-10657, Dubna, 1977.
[8]V. K. Suslenko and I. I. Haysak, JINR Preprint R2-83-298,Dubna, 1983.
[9]L. S. Azhgireĭ and V. P. Chizhikov, JINR Preprint R2-4937, Dubna, 1971; L. S. Azhgireĭ *et al.*, Yad Fiz. **13**, 581 (1971) [Sov. J. Nucl. Phys. **13**, 328 (1971)].
[10]I. I. Haysak and V. K. Suslenko, JINR Preprint R2-83-348,Dubna, 1983.
[11]F. H. Cverna *et al.*, Phys. Rev. C **23**, 1698 (1981).
[12]V. K. Suslenko, Fiz. Elem. Chastits, At. Yadra **6**, 173 (1973) [Sov. Phys. Part. Nucl. **6**, 70 (1975)].
[13]M. Gell-Mann and K. M. Watson, Ann. Rev. Nucl. Sci. **4**, 219 (1954).
[14]A. G. Meshkovskiĭ, Ya. Ya. Shalamov, and V. A. Shebanov, Zh. Eksp. Teor. Fiz. **35**, 64 (1958) [Sov. Phys—JETP **8**, 46 (1959)].
[15]M. G. Meshcheryakov *et al.*, Zh. Eksp. Teor. Fiz. **31**, 45 (1956) [Sov. Phys—JETP **4**, 60 (1957)].
[18]V. G. Vovchenko, Dokl. Akad. Nauk SSSR **163**, 1348 (1965) [Sov. Phys.—Dokl. **10**, 761 (1966)].
[17]A. G. Meshkovskiĭ *et al.*, Zh. Eksp. Teor. Fiz. **31**, 560 (1956 [Sov. Phys.—JETP **4**, 404 (1957)].
[18]V. G. Vovchenko *et al.*, Zh. Eksp. Teor. Fiz. **39**, 1557 (1960) [Sov. Phys.—JETP **12**, 1084 (1961)].
[19]B. S. Neganov and O. V. Savchenko, Zh. Eksp. Teor. Fiz. **32**, 1265 (1957) [Sov. Phys.—JETP **5**, 1033 (1957)].
[20]V. V. Abayev *et al.*, LITaF Preprint #569, USSR Academy of Sciences, 1980.
[21]B. J. Verwest, Phys. Lett. **83B**, 161 (1979).
[22]J. Hudomalj-Gabitzsch *et al.*, Phys. Rev. C **18**, 2666 (1978).

Translated by Gregory Toker